ACTA METALLURGICA SLOVACA
2021, VOL. 27, NO. 4, 190-194

RESEARCH PAPER

EFFECT OF PLASMA NITRIDING OF AUSTENITIC STAINLESS STEEL PRODUCED BY DIRECT METAL LASER SINTERING

Dorina Kovács[1], Dávid Miklós Kemény[1]*

[1] Department of Materials Science and Engineering, Faculty of Mechanical Engineering, Budapest University of Technology and Economics, Budapest, Hungary 1111, Budapest, Műegyetem rakpart 3

*Corresponding author: kovacs.dorina@gpk.bme.hu, tel.: +361463-1079, Budapest University of Technology and Economics, Hungary 1111, Budapest, Műegyetem rakpart 3

Received: 17.09.2021
Accepted: 18.11.2021

ABSTRACT

The additive manufacturing (AM) is a technology that produces 3D workpieces using a wide range of different metals as raw materials. The aim of current research is to investigate the plasma nitriding effect on the Direct Metal Laser Sintering (DMLS) produced samples. The direct current plasma nitriding treatment was achieved at 440 °C for 4 hours with 75 % N_2 – 25 % H_2 gas mixture. Before the treatment, the 316L austenitic stainless steels samples were ground with different methods to modify the surface roughness. Scanning electron microscope (SEM), X-ray diffractometer, glow discharge optical electron spectroscopy, Vickers microhardness tester and potentiodynamic corrosion test were used for the characterization of surface properties. The results demonstrated that the surface roughness did not affect the outcome of the plasma nitriding.

Keywords: additive manufacturing, DMLS, austenitic stainless steel, plasma nitriding, corrosion rate

INTRODUCTION

Due to technology development, there are more and more opportunities to create materials with different geometries. Not only development within traditional subtractive processes exists, but also within additive processes. The latter technology is widely used in industries, universities, and medicines. This is due to the relatively slow production, cost-efficient, precise dimensional accuracy, and customizable geometry. In addition, the finished product does not need other manufacturing processing, but heat treatment is necessary [1–5].

For all AM (Additive Manufacturing) equipment, user-level knowledge of a CAD (Computer Aided Design) program is needed to create a model of the desired product, even with sufficiently complex geometry. Based on the model, the product can be built layer-by-layer [6,7,8].

In our research, 316L type stainless steel was produced with Direct Metal Laser Sintering (DMLS). The DMLS procedure starts by applying a thin layer of powder material to the building platform. After each layer, a laser beam fuses the powder at exactly the points defined by the model [9]. When one layer is done, the platform is lowered, and another layer of powder is applied. At the point of the laser beam impact, the metallic powder is locally melted, whereby the underlying layer is over melted and then solidified [10–13]. This continues until the product will be done. The thickness of one powder layer is between 0.020 to 0.100 mm [14]. The major concern of the DMLS process is the building time. Parts of even small-moderate size may require more than 6-12 hours of processing. Another concern is the part accuracy, which also needs to be kept as high as possible. Minimizing the build time can reduce the surface accuracy and vice versa [15]. Other disadvantages of the technology are the porosity and the significant microstructure defects, but these can be reduced by optimizing the parameters [16].

The procedure of the AM parts is well-researched area, but the surface treatment may cause differences from the traditional manufacturing technologies because of the different structure and surface integrity. One of the main groups of surface treatment is nitriding.

Low temperature plasma nitriding provides excellent wear resistance with high surface hardness without decreasing the corrosion resistance [17]. At this temperature (≤450 °C), the formation of chromium-nitride is inhibited [18-21]. During the nitriding of austenitic stainless steel, a diffusion layer is formed on the surface, which is known as S phase. If the nitriding temperature is increasing, these precipitations result in the depletion of free Cr, which causes lower corrosion resistance of the surface. At higher temperatures, Cr and Fe_4N phases can be formed, which improved the wear resistance because of the higher hardness than that of the S-phase [22–24]. Although the wear resistance increases with the nitriding temperature, the corrosion resistance decreases. This type of 316L steel is mainly used in many industries and the fields of biomaterials [25-27]. Lin et al. investigated the antibacterial rate to recognize the antibacterial effect of the S phase. The test showed that the untreated sample did not possess any antibacterial property, but the nitrided samples displayed excellent results [28], which was proven by other research groups [29,30]. A biocompatibility test was carried out by Martinesi et al. in collagen-coated nitrided steel. They concluded that nitriding and collagen coating could improve the biocompatibility of endothelial cells [31]. Heras et al. said the low nitrogen content caused higher corrosion resistance [32].

Austenitic stainless steels are commonly used metallic materials for AM because there is no martensitic phase transformation [33–36]. A few years ago, coatings of additively manufactured samples were getting come into focus.

Kovaci and Secer [37] plasma nitrided an L-PBF manufactured samples at 400 °C for 2 hours with 50-50 % H_2-N_2 gas mixture. Different patterns (triangle, hexagonal, ellipse) were created

from the base 316L powder. The plasma treatment increased the surface roughness and the friction coefficient because of the created hard abrasive particles.
Funch et al. [38] also used L-PBF to create 316L samples for high temperature solution nitriding (HTSN). It was carried out at 1100 °C for 2 hours at N_2 pressure of 300 mbar. The aim was not to create a nitrided layer, only use the solid solution strengthening effect of nitrogen. The high temperature treatment occurred in the loss of the cellular structure and fusion boundaries. Godec et al. [39] adopted both the solution treating to eradicate the residual stresses and nitriding. The specimens were nitrided at 430 °C for 15 hours in a 75%H_2 – 25%N_2 gas mixture. The AM specimen hardness was higher because of the residual stresses and the higher dislocation density. After nitriding, the wear volume was significantly decreased against other research [40], and rather the corrosion properties were better than the commercial material.
The aim of this research is to combine the DMLS technology and plasma nitriding. Properties of different surface roughness were investigated to better understanding the effect of the treatment.

MATERIAL AND METHODS

Sample preparation

316L stainless steel was used for the investigations with the following chemical composition shown in **Table 1**. The EOS M100 type of AM equipment was used to produce the samples. The samples were made by DMLS in 20×30×6 size. The technical parameters are the following: the building area is ø100 mm and 95 mm high; the laser type is Yb-fiber laser with 40 µm focus diameter, adjustable 200 W laser performance and 7 m/s scanning speed. Our samples were produced with 71 W laser performance and 0.82 m/s scanning speed.

Table 1 Measured chemical composition of 316L (in w%) compared with the given percentages by EOS and measured by EDS

	EOS	Produced
Fe	bal.	bal.
Cr	17-19	20.06
Ni	13-15	12.79
Mo	2.25-3	2.41
C	<0.03	0.00
Mn	<2	1.51
Cu	<0.5	0.00
P	<0.025	0.00
S	<0.01	0.02
Si	<0.75	1.32

For the examinations, four samples were produced with the same additive process. The surface preparation of the samples was different, which is shown in **Table 2**. During the solidification, 30 µm splats were created, which caused an uneven surface. Because of this phenomenon, four samples were used with different surface roughness for the experiments. The samples were ground with different SiC paper.

Table 2 Surface roughness of the samples with the number of the SiC paper

Sample	Grit Number	Ra (µm)
N0	originally produced	2.5
N1	80	1.6
N2	280	0.55
N3	4000	0.01

Plasma nitriding

The experiments of the direct current plasma nitriding were made in customized laboratory equipment. The nitriding process was carried out at 440 °C for 4 hours with 75 % N_2 – 25 % H_2 gas mixture at 2.8 mbar. Before the treatment, the chamber was rinsed with argon gas. The 4 hours nitriding time started when the sample reached the proper temperature. After the process, the air was introduced into the chamber, and the samples cooled down to room temperature. The temperature was measured by using an isolated K-type thermocouple under the workpiece.

Characterization methods

The hardness of the nitrided samples was measured with Vickers microhardness tester (Buehler IndentaMet 1105, 50g load). After the etching with Aqua Regia, the cross-sections of the samples were observed by Zeiss EVO MA10 scanning electron microscope (SEM). The composition depth profile was analyzed using a Spectruma GDA Alpha Glow Discharge Optical Emission Spectroscopy (GDOES). The chemical composition was measured with Energy-dispersive X-ray spectroscopy (EDS) of SEM. The analysis of the created phases on the layer were performed with PANalytical X'pertPro MPD X-ray diffractometer using an X'celerator type detector with Cu Kα radiation, the scan parameters were 0°-90° in 2 thetas, the wavelength was 1.54 nm, while the exposure time was set to 0.3 s/step. The corrosion resistance of the samples was evaluated by measuring polarization curves in 3.5 % NaCl solution using BioLogic SAS type SP-150 electrochemical working station. The working electrode was a Hg_2Cl_2/KCl calomel electrode as the reference electrode and platinum was used as the counter electrode.

RESULTS AND DISCUSSION

Microstructure and hardness

Fig. 1 shows the surface of the samples before and after the nitriding. It is seen in Fig. 1 a-b), the DMLS manufacturing system created 30 µm spheres during the solidification, which caused an uneven surface. It is also observed especially in Fig. 1 g-h), the plasma nitriding caused a rougher surface than the original because of the nitrogen bombardment.

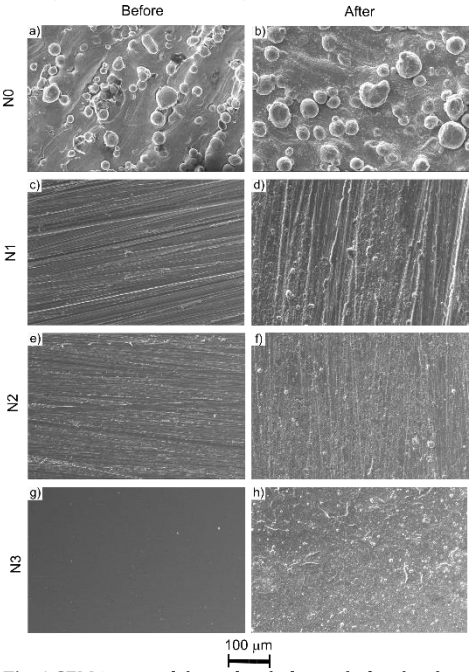

Fig. 1 SEM images of the surface before and after the plasma nitriding. The roughness of the surface a-b) 2.5, c-d) 1.6 e-f) 0.55 g-h) 0.01 µm.

This surface area modification is negligible compared to the unground surface. This increased area will have been important during the corrosion measurements.
The nitrided layer and the hardness profile obtained from the cross-sections of the nitrided sample surfaces are given in Fig. 2. The hardness values of the untreated sample were measured as 250 HV0.05. The hardness profiles provide comprehensive images about the hardness compared with the depth of nitrided layers. The results show the hardness is even along the nitrided layer, then the hardness decreased to the substrate hardness under the modified layer. The expanded austenite, called S-phase, has high hardness due to lattice distortion caused by interstitial nitrogen atoms. It reduces the mobility of dislocations and improves the mechanical properties of the layer [41]. **Table 3**. shows the maximum together with the formed layer thickness.

Table 3 Layer thickness and maximum hardness of the treated samples

Sample	Layer thickness (μm)	Maximum hardness (HV0.05)
N0	43	950
N1	44	910
N2	44	860
N3	43	1100

The layer thickness of the specimens is the same, while the maximum hardness is different. It depends on the nitrogen content of the layer. If the concentration of the nitrogen increases, more reticular distortion causes a higher hardening effect [42].

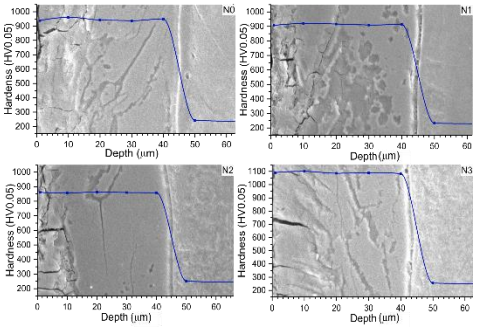

Fig. 2 SEM images of the nitrided layer and the hardness profile of the samples

Characteristic of the layer
The XRD measurements were performed on the top of the created layer, which can be seen in **Fig. 3**. As it can be observed, γ_N is considered to be a saturated solid solution of nitrogen in the austenitic phase. Besides this, CrN and Fe_4N were created, which means that the temperature was not enough low to avoid this phase. **Fig. 2** also referred to this phase because on the microstructure images, the layer is not even, there is some dark area through the zone.
The depth profiles of the nitrogen concentration are presented in **Fig. 4**. The trends of the profiles are similar to each other. They have a plateau-shapes. In this case, a slowly decrease can be observed from the surface that followed by a rather sharp leading edge [43]. The N3 sample has the highest nitrogen content, which corresponds to the hardness value. The diffusion depth measured by GDOES is consistent with the scanning electron microscopy micrographs. The nitrogen is decreasing from the surface to the base nitrogen content as 19 at%. According to the results, the previous surface preparation did not influence the nitrogen diffusion to the material.

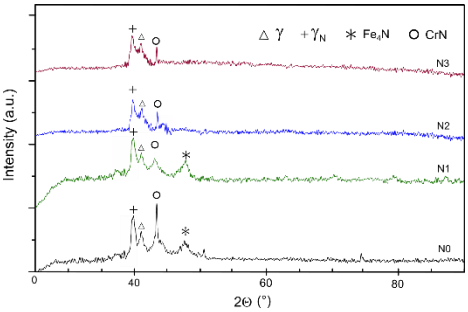

Fig. 3 XRD pattern of nitrided layer on AISI 316 austenitic stainless steel

Corrosion test
Tafel plots were used to resolve the corrosion resistance of the plasma nitrides (N0, N1, N2, N3) and untreated samples. The samples were measured in 3.5 % NaCl solution for 24 hours which were plotted in Fig. 5. The Tafel extrapolation was used to determine the corrosion potential and current density. The corrosion rate was calculated from these values according to McCafferty [44] and ASTM G102 standard. Table 4. summarised the corrosion parameters. A Stern-Geary equation [45] was used to calculate the polarization resistance (Rp) [46]

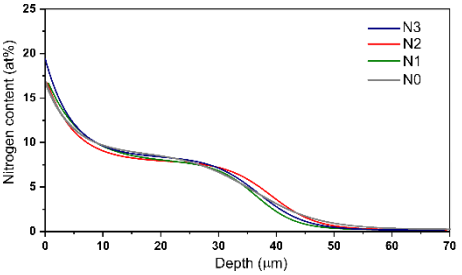

Fig. 4 Nitrogen content of the nitrided layers on AISI 316 austenitic stainless steel

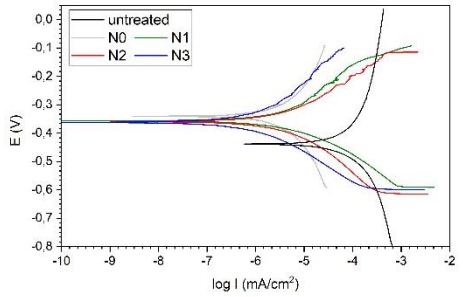

Fig. 5 Polarization curves of untreated and plasma nitrided samples after 24h in 3.5% NaCl solution

It can be seen, the nitrided samples have higher corrosion potential (Ecorr = -0.36…(-0.34) V) and lower corrosion current density (icorr ~ 3…5 μA/cm^2)) than the untreated sample (Ecorr = - 0.44 V and icorr = 21.7 μA/cm^2) which indicated a better corrosion resistance after the plasma nitriding.
The corrosion rate differs greatly between untreated and nitride specimens. The corrosion rates are similar, but a slight difference can be observed. The untreated sample has the highest corrosion rate. Among the nitrided specimens, the N3 sample

has the best polarization resistance as it can be seen in Table 4. The specific surfaces of the samples are different because of the preparation method. The untreated sample has the highest surface because the original solidification parts can increase the area. The increased surface area can affect the corrosion, while the other samples have a similar.

CONCLUSION

The surface treatment of the additive manufactured parts is an important factor during the process. In this research, plasma nitriding was used to investigate the effects on the DMLS produced surface. Although the surface roughness was different in each sample, neither the formed layer thickness nor the depth of the diffused nitrogen was not changed. The CrN was created on the layer, which was caused by the closeness of the formation temperature. The corrosion rate was five times higher by/in the untreated sample as the nitrided ones. There is no significant difference in the corrosion rate of the nitrided specimen. It can be stated that as the surface roughness decreases, the corrosion rate also decreases. So, the better surface roughness results a better corrosion resistance increases.

Table 4 Corrosion parameters

Sample	i_{corr} ($\mu A/cm^2$)	E_{corr} (V)	β_a (mV/dec.)	β_c (mV/dec.)	corr.rate (mm/year)	Rp ($10^3\Omega cm^2$)
untreated	21.709	-0.439	144	107	0.098	1.229
N0	4.947	-0.341	321	342	0.022	14.547
N1	5.042	-0.356	870	778	0.021	35.396
N2	4.942	-0.359	665	924	0.018	33.979
N3	2.947	-0.363	909	566	0.013	51.428

Acknowledgments: The research reported in this paper was supported by Department of Automotive Technologies, Budapest University of Technology and Economics. The authors are also grateful to dr. János Madarász for the XRD measurements. The research reported in this paper and carried out at BME has been supported by the NRDI Fund (TKP2020 IES, Grant No. BME-IE-NAT and TKP2020 NC, Grant No. BME-NC) based on the charter of bolster issued by the NRDI Office under the auspices of the Ministry for Innovation and Technology.

REFERENCES

1. B. Anush Raj, J.T. Winowlin Jappes, M. Adam Khan, V. Dillibabu, N.C. Brintha: Optik, 202, 2020, 163735. https://doi.org/10.1016/j.ijleo.2019.163735.
2. A. Gebhardt: *Understanding Additive Manufacturing*. Munich: Hanser Publications, 2011.
3. G.G. Arias, F.J. Díaz, E.R. Ramirez, J.V. Guzman: Periodica Polytechnica Mechanical Engineering, 65, 2021, 129–133. https://doi.org/10.3311/PPme.16203.
4. Z. Keresztes, D. Pammer, J.P. Szabo: Periodica Polytechnica Mechanical Engineering, 63, 2019, 195–20, https://doi.org/10.3311/PPme.13821.
5. C.S. Lefky, B. Zucker, D.Wright, A.R. Nassar, T.W. Simspon, O.J. Hildreth: 3D Printing and Additive Manufacturing, 4, 2017, 3–11. https://doi.org/10.1089/3dp.2016.0043.
6. M. Chimmat, D. Srinivasan: Procedia Structural Integrity, 14, 2019, 746–757. https://doi.org/10.1016/j.prostr.2019.05.093.
7. R. Konečná, G. Nicoletto, S. Fintová, M. Frkáň: Procedia Structural Integrity, 7, 2017, 92–100. https://doi.org/10.1016/j.prostr.2017.11.065.
8. A. Saboori, A. Aversa, F. Bosio, E. Bassini, E. Librerab, M. De Chirico, S. Biamino, D. Ugues, P. Fino, M. Lombardi: Materials Science & Engineering A, 766, 2019, 138360. https://doi.org/10.1016/j.msea.2019.138360.
9. R. Bidulsky, J. Bidulska, F.S. Gobber, T. Kvackaj, P. Petrousek, M. Actis-Grande, K.-P. Weiss, D. Manfredi: Materials, 13, 2020, 3328. https://doi.org/10.3390/ma13153328.
10. J.S. Cuellar, G. Smit, D. Plettenburg, A. Zadpoor: Additive Manufacturing, 21, 2018, 150–158. https://doi.org/10.1016/j.addma.2018.02.004.
11. P. Dong, F. Vecchiato, Z. Yang, P.A. Hooper, M.R. Wenman: Additive Manufacturing, 40, 2021, 101902. https://doi.org/10.1016/j.addma.2021.101902.
12. K. Bán, M. Nagy, Z. Fogarassy, A. Szabó: Acta Physica Polonica A, 137, 2020, 861–863. https://doi.org/10.12693/APhysPolA.137.861.
13. M. Shehata, T.M. Hatem, W.A. Samad: 3D Printing and Additive Manufacturing, 6, 2019, 227–233. https://doi.org/10.1089/3dp.2017.0106.
14. A. Guzanová, G. Ižaríková, J. Brezinová, J. Živčák, D. Draganovská, R. Hudák: Metals, 7, 2017, 318. https://doi.org/10.3390/met7080318.
15. A. Verma, S. Tyagi, K. Yang: The International Journal of Advanced Manufacturing Technology, 77, 2015, 847–860. https://doi.org/10.1007/s00170-014-6443-x.
16. A. E. Patterson, S. L. Messimer, P. A. Farrington: Technologies, 5, 2017, 15. https://doi.org/10.3390/technologies5020015.
17. T.V. Trinh, T.H. Pham, H.T. Nguyen, T.V. Nguyen: Acta Metallurgica Slovaca, 25, 2019, 276-282. https://doi.org/10.12776/ams.v25i4.1356.
18. P. Petrousek, T. Kvackaj, R. Kocisko, J. Bidulska, M. Luptak, D. Manfredi, M.A. Grande, R. Bidulsky: Acta Metallurgica Slovaca, 25, 2019, 283-290. https://doi.org/10.12776/ams.v25i4.1366.
19. X. Zhang, J. Wang, H. Fan, D. Pan: Applied Surface Science. 440, 2018, 755-762. https://doi.org/10.1016/j.apsusc.2018.01.225.
20. J. Biehler, H. Hoche, M. Oechsner: Surface & Coatings Technology. 313, 2017, 40–46. https://doi.org/10.1016/j.surfcoat.2017.01.050.
21. L. Gil, S. Brühl, L. Jiménez, O. Leon, R. Guevara, M.H. Staia: Surface & Coatings Technology, 201, 2006, 4424–4429. https://doi.org/10.1016/j.surfcoat.2006.08.081.
22. A. F. Yetim, M. Yaz: Journal of Bionic Engineering, 11, 2014, 620–629. https://doi.org/10.1016/S1672-6529(14)60073-1.
23. I. Braceras, I. Ibáñez, S. Dominguez-Meister, J. A. Sánchez-García, B.A. Larrañaga, I. Garmendia: Surface & Coatings Technology, 355, 2018, 116–122. https://doi.org/10.1016/j.surfcoat.2018.04.057.
24. M. Naeem, M. Shafiq, M. Zaka-ul-Islam, N. Nawaz, J.C. Díaz-Guillén: Materials Letter, 181, 2016, 78–81. https://doi.org/10.1016/j.matlet.2016.05.144.
25. D. Károly, D. Charalambous, B. Pogácsás, T. Micsik, C. Barile, K. Casavola: Materials Today: Proceedings, 3, 2016, 997–1002. https://doi.org/10.1016/j.matpr.2016.03.036.
26. T. Hryniewicz, R. Rokicki, K. Rokosz: Surface & Coatings Technology, 202, 2008, 1668–1673. https://doi.org/10.1016/j.surfcoat.2007.07.067.
27. A. Aversa, G. Marchese, E. Bassini: Metals, 11, 2021, 932. https://doi.org/10.3390/met11060932.
28. L. Lin, S. Chen, C. Wu, J. Hung, K. Ou: Applied Surface Science, 257, 2011, 7375–7380. https://doi.org/10.1016/j.apsusc.2011.01.065.
29. K. Ou, H. Chou, C. Liu, P. Peng: Surface & Coatings

Technology, 206, 2011, 1142–1145.
https://doi.org/10.1016/j.surfcoat.2011.08.001.
30. C. F. Hung, C. Z. Wu, W. F. Lee, K.L. Ou, C.M. Liu, P.W. Peng: Physics Procedia, 32, 2012, 914–919. https://doi.org/10.1016/j.phpro.2012.03.656.
31. M. Martinesi, M. Stio, C. Treves, F. Borgioli: Materials in Medicine, 24, 2013, 1501–1513.
https://doi.org/10.1007/s10856-013-4902-9.
32. E. D. Heras Las, G. Ybarra, D. Lamas, A. Cabo, E.L. Dalibon, S.P. Brühl: Surface & Coatings Technology, 313, 2017, 47-54.
https://doi.org/10.1016/j.surfcoat.2017.01.037.
33. J. R. Trelewicz, G. P. Halada, O. K. Donaldson, G. Manogharan: The Minerals, Metals & Materials Society, 68, 2016, 850–859.
https://doi.org/10.1007/s11837-016-1822-4.
34. D. Gu, Y. Shen: Applied Surface Science, 255, 2008, 1880–1887. https://doi.org/10.1016/j.apsusc.2008.06.118.
35. E. Kalácska, B. Varbai, J. Ginsztler, K. Májlinger: IOP Conference Series: Materials Science and Engineering, 426, 2018, 012021.
https://doi.org/10.1088/1757-899X/426/1/012021.
36. B. Tegze, E. Albert, B. Dikó, J. Madarász, Gy. Sáfrán, Z. Hórvölgyi: Studia Universitatis Babes-Bolyai Chemia, 64, 2019, 81–98.
http://doi.org/10.24193/subbchem.2019.3.07.
37. H. Kovaci, Y. Seçer: Surface & Coatings Technology, 400, 2020, 126178. https://doi.org/10.1016/j.surfcoat.2020.126178.
38. C. V. Funch, T. L. Christiansen, M.A.J. Somers: Surface & Coatings Technology, 403, 2020, 126385. https://doi.org/10.1016/j.surfcoat.2020.126385.
39. M. Godec, C. Donik, A. Kocijan, B. Podgornik, D.A. Skobir Balantič: Additive Manufacturing, 32, 2020, 101000.
https://doi.org/10.1016/j.addma.2019.101000.
40. G. C. Mondragón-Rodríguez, N. Torres-Padilla, N. Camacho, D.G. Espinosa-Arbeláez, G.V. de León-Nope, J.M. González-Carmona, J.M. Alvarado-Orozco: Surface & Coatings Technology, 387, 2020, 125526.
https://doi.org/10.1016/j.surfcoat.2020.125526.
41. M. G. Shahri, S. R. Hosseini, M. Salehi, M. Naderi: Surface & Coatings Technology, 296, 2016, 40–45. https://doi.org/10.1016/j.surfcoat.2016.03.058.
42. A. Fossati, F. Borgioli, E. Galvanetto, T. Bacci: Surface & Coatings Technology, 200, 2006, 3511–3517.
https://doi.org/10.1016/j.surfcoat.2004.10.122.
43. T. Moskalioviene, A. Galdikas: Vacuum, 86, 2012, 1552–1557.
https://doi.org/10.1016/j.vacuum.2012.03.026.
44. E. McCafferty: Corrosion Science, 47, 2005, 3202–3215.
https://doi.org/10.1016/j.corsci.2005.05.046.
45. D. B. Matthews: Australian Journal of Chemistry, 28, 1975, 243–251. https://doi.org/10.1071/CH9750243.
46. K. Turalıoğlu, M. Taftalı, H. Tekdir, O. Comakli, M. Yazici, T. Yetim et al.: Surface & Coatings Technology, 405, 2021, 126635.
https://doi.org/10.1016/j.surfcoat.2020.126635.